Structure Development in Melt Spinning of Poly(ethylene-*co*-octene) Filaments with Various Comonomer Contents

Haifeng Shan, James L. White

Institute of Polymer Engineering, University of Akron, Akron, Ohio 44325

Received 6 November 2003; accepted 23 January 2004
DOI 10.1002/app.20333
Published online in Wiley InterScience (www.interscience.wiley.com).

ABSTRACT: An experimental study of the spinnability and the variation in crystallinity and orientation of melt spinning of poly(ethylene-*co*-octene) with different contents of comonomers was carried out. The spinning behavior of these polymers was investigated under different draw-down ratios and temperatures and correlated to spinline stress. The melt-spun filaments were characterized by wide-angle X-ray diffraction birefringence, and differential scanning calorimetry. S-1 is a high-density polyethylene and S-2, S-3, and S-4 have 16, 22, and 38 wt % octene. An orthorhombic unit cell was found in all four polymers, but a dominant hexagonal structure (perhaps mesophase) was found for the highest octene level (S-4). The orientation factors for the *a*-, *b*-, and *c*-axis of the orthorhombic crystal structure and *a*-axis of the hexagonal phase were then calculated. The crystalline orientation behavior of the lower octene copolymers (S-1, S-2, and S-3) are similar and can be represented as a "row-nucleated" structure. However, the orientation behavior of S-4 was different. The uniaxial mechanical properties were also measured. The Young's modulus and tensile strength generally increased with birefringence for all polymers. With increasing content of octene, the Young's modulus showed a decrease from semicrystalline thermoplastic toward an elastomer. © 2004 Wiley Periodicals, Inc. J Appl Polym Sci 93: 9–22, 2004

Key words: poly(ethylene-*co*-octene); crystal structures; orientation; WAXD; differential scanning calorimetry (DSC)

INTRODUCTION

There is long history of investigations of structure development in melt spinning polyethylene fibers,[1–8] which is almost completely involved with high-density polyethylene (HDPE) containing little comonomer or long chain branching. These studies reported orthorhombic[9] polyethylene crystals formed in the spinline. In recent years, there has been an increasing number of articles[10–21] describing the characteristics of polyethylene copolymers with high comonomer contents, especially octene-1, but still containing substantial levels of crystallinity. Both the orthorhombic phase[9] and a hexagonal phase[16,17] have been found.

In the present article, we considered structure development in melt spinning of polyethylene copolymers. We melt-spun fibers under known draw-down ratio and spinline stress conditions. The melt-spun fibers were examined by the wide-angle X-ray diffraction (WAXD) and by birefringence. The primary investigative focus was given to the crystallographic structures formed and to polymer chain/crystallographic axis orientation and crystallinity levels. Mechanical properties were also studied.

Correspondence to: J. White.

Journal of Applied Polymer Science, Vol. 93, 9–22 (2004)

EXPERIMENTAL

Materials

The polyethylene copolymers considered in this study, summarized in Table I, are four in number, with densities varying from 0.870 to 0.958 g/cm^3. S-2, S-3, and S-4 are ethylene–octene copolymers prepared by Dow's Insite® constrained geometry catalyst (CGCT) and process technology, which can impart a material narrow molecular weight distribution, homogeneous comonomer distribution, and a controlled branching structure. S-1 is a conventional HDPE synthesized with a Ziegler–Natta catalyst.

Material characterization

Thermogravimetric characterization

Thermogravimetric analysis (TGA) of the various samples was investigated using a TA Instruments (New Castle, DE) TGA 2050 at the heating rate of 20°C/min over the temperature range from room temperature to 700°C under N_2 atmosphere. The TGA scans are shown in Figure 1.

It is evident from the figure that these four samples are neat polymers without any fillers and similar minimal additives, given that their weight loss (%) goes to zero after complete burning. We can also see that all four materials are degraded at about 480°C, which suggests their thermal stability is essentially the same.

TABLE I
Characterization Data of Copolymers Used in This Study

Property	Polymer designation			
	S-1	S-2	S-3	S-4
Density (g/cm^3)[22]	0.958	0.916	0.902	0.870
Type of comonomer[22]	None	Octene	Octene	Octene
Content of comonomer (wt %)[22]	0	15	20	38
Calculated content of comonomer (mol %)	0	4.2	5.9	13.3
Catalyst	Ziegler–Natta	Dow Insite®	Dow Insite®	Dow Insite®
MI (g/10 min)[22]	0.95	1.00	1.00	5.00
M_w[a]	1.70×10^5	1.45×10^5	1.52×10^5	0.90×10^5
Grade	Alathon M6210	Elite 5400	Affinity PL1880	Engage 8200
Manufacturer	Equistar	Dow	Dow	DuPont Dow

[a] Estimated from the shear viscosity data using correlations from Wood-Adams et al.[32] and Raju et al.[33]

Differential scanning calorimetry

Differential scanning calorimetry (DSC) studies were carried out on the as-received samples with a Perkin–Elmer DSC-7 (Perkin Elmer Cetus Instruments, Norwalk, CT). The samples were first melted to eliminate the influence of their production origins and then cooled to −30°C at a cooling rate of 10°C/min. Subsequently, samples were heated at a heating rate of 10°C/min under N_2 atmosphere. DSC scans are depicted in Figure 2. The degree of crystallinity and the melting point of each material are summarized in Table II.

We can see from Table II that the higher the content of comonomer, the lower the melting point, the crystallinity of the polymer, and the broader the melting peak.

Melt viscosity

An Advanced Rheometric Expansion System (ARES, Rheometric Scientific, Inc., Piscataway, NJ) was used in the oscillatory mode with parallel-plate fixtures (25 mm diameter). Dynamic frequency sweep experiments were conducted. The complex viscosity (η^*) was measured as a function of angular frequency (ω), ranging from 0.01 to 100 rad/s at 180°C for all four polymers. The data are summarized in Figure 3. We used the Cox–Merz rule[23] [$\eta^*(\omega) = \eta(\dot{\gamma})$], which was found to be valid by earlier investigators[24–31] for polyethylene and its copolymers, to obtain the steady shear viscosity. η_0 gives information about the zero shear viscosity. From Wood-Adams et al.[32] and Raju et al.,[33] we can estimate the weight-average molecular weight, which is given in Table I. A Vinogradov–Malkin[34] reduced viscosity plot of η/η_0 versus $\eta_0\dot{\gamma}$ was constructed to study the molecular weight distribution. It is known that η/η_0 decreases more rapidly for broader molecular weight distribution polymer.[35–37] We depict such a plot in Figure 4, which suggests the molecular weight distribution broadness as follows: S-1 > S-3 > S-2 > S-4. Apparently, S-1, which was synthesized with Ziegler–Natta catalyst,

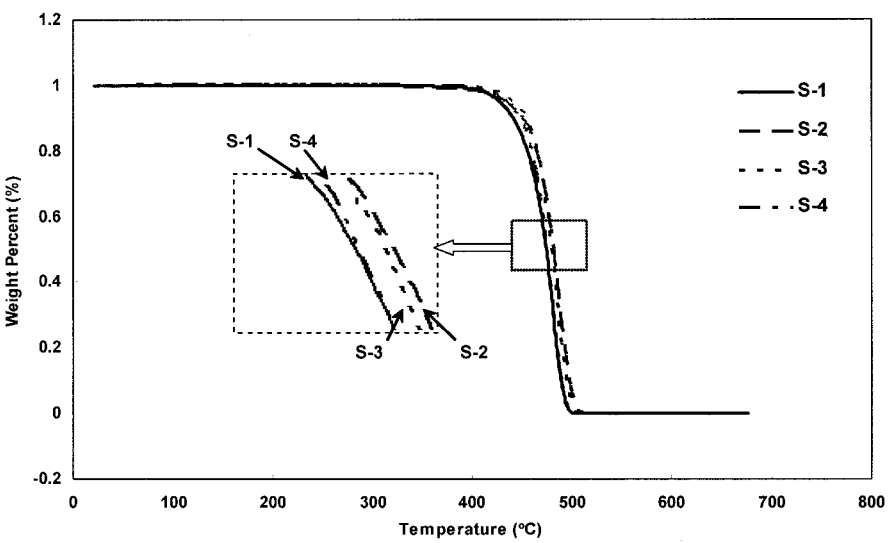

Figure 1 Thermogravimetric analysis of as-received copolymers at a heating rate of 20°C/min.

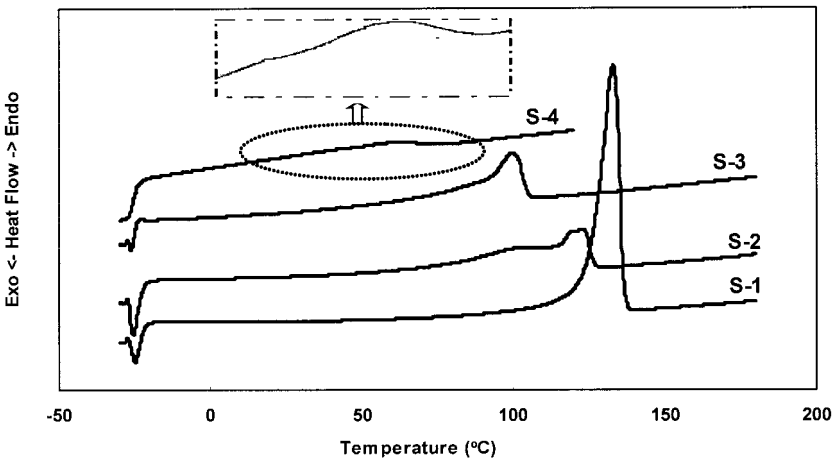

Figure 2 DSC thermograms of as-received copolymers measured at a heating rate at 10°C/min.

has a broader molecular weight distribution than that of S-2, S-3, and S-4, which were synthesized with the Dow Insite® catalyst.

Melt-spinning process

The four polymers were melt spun as monofilament from an Instron (Canton, MA) capillary rheometer, with a capillary die of diameter 1.6 mm and length–diameter ratio of 19.3. Experiments were carried out at 170°C for all four polymers and at selected individual temperatures for each. In particular, we conducted experiments at 180, 170, and 150°C for S-1; at 210, 190, and 170°C for S-2; at 190, 170, and 150°C for S-3; and at 170, 150, and 130°C for S-4. The extruded filament was taken up on a bobbin at various velocities. Draw-down ratios up to 1300 were investigated. The spinning path for the taken-up fiber was approximately 900 mm.

An electronic tensiometer (Rothschild R-1192) was used to measure the filament spinline tensions.

Structure characterization of fibers

The crystallinities of melt-spun filaments were measured using Perkin–Elmer DSC-7 at a heating rate of 10°C/min under nitrogen atmosphere.

TABLE II
Melting Point, Heat of Fusion, and Crystallinity of As-Received Copolymer

Property	Polymer designation			
	S-1	S-2	S-3	S-4
Melting point (°C)	133.0	122.9	99.9	57.7
Heat of fusion (J/g)	204.4	104.6	82.0	47.9
Crystallinity (%)[a]	70.5	36.1	28.3	16.5

[a] Using 290 J/g as the heat of fusion of the crystalline phase of polyethylene.

The crystalline form in the filaments was characterized by WAXD film patterns, obtained using a General Electric X-ray generator (GE-XRD6; Milwaukee, WI), equipped with a copper target tube. A graphite crystal monochrometer was used to obtain the Cu–K_α radiation (λ = 0.15418 nm). The operation voltage and current were 30 kV and 30 mA, respectively.

We also sought to determine polymer chain and crystallographic axis orientation factor. Hermans and Plazek,[38] and subsequently F. Muller,[39] proposed a measure of the average orientation of polymer chains relative to the axis of a fiber in which there is complete molecular symmetry around the axis. Muller formulates this as

$$f_H = \frac{\alpha_z - \alpha_r}{\alpha_\parallel - \alpha_\perp} \tag{1}$$

where α_z and α_r are the polarizabilities parallel and perpendicular to the fiber axis and $\alpha_\parallel$ and $\alpha_\perp$ are the polarizabilities along and perpendicular to the polymer chain, respectively. It was shown that

$$f_H = \tfrac{1}{2}[3\ \overline{\cos^2\Phi} - 1] \tag{2}$$

where Φ is the angle between the polymer chain axis and the fiber axis and $\overline{\cos^2\Phi}$ indicates an average over all the polymer chains around the solid angle. For the case of complete parallel alignment of chains with the fiber axis, Φ is zero and f_H becomes unity. For the case of chains aligned perpendicular to the fiber axis, Φ is 90°, and f_H is -0.5. Stein[40] later pointed out that eq. (2) may be generalized for a crystalline polymer so as to include all three crystallographic axes:

$$f_a = \tfrac{1}{2}[3\ \overline{\cos^2\Phi_{a,z}} - 1] \tag{3a}$$

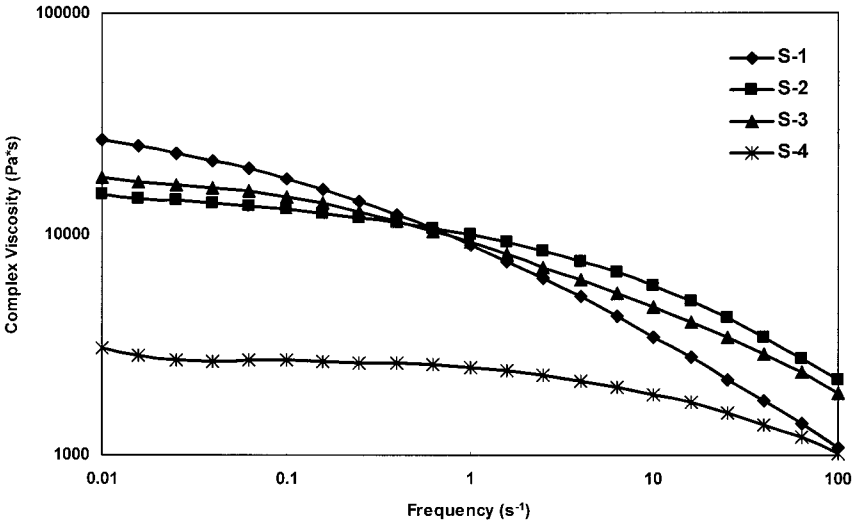

Figure 3 Complex viscosities of four polymers at 180°C.

$$f_b = \tfrac{1}{2}[3\ \overline{\cos^2\Phi_{b,z}} - 1] \tag{3b}$$

$$f_c = \tfrac{1}{2}[3\ \overline{\cos^2\Phi_{c,z}} - 1] \tag{3c}$$

where $\Phi_{a,z}$, $\Phi_{b,z}$, and $\Phi_{c,z}$ (defined by Fig. 5) represent the angles formed by the *a*, *b*, and *c* crystallographic axes. The *c*-axis orientation factor corresponds to the Hermans orientation factor. For an orthorhombic unit cell such as existing in polyethylene, Stein[40] shows that the orthogonality requires

$$f_a + f_b + f_c = 0 \tag{4}$$

Hermans and Platzek[38] proposed measuring f_c by birefringence. Hermans et al.[44] later proposed the use of WAXD but applied it only to cellulose rayon. Subsequently, Stein[40] applied WAXD to determine the crystalline orientation factors of eq. (3) for polyethylene using the (200) and (020) planes. We found the diffraction arc of the (020) plane, especially for low-density polyethylenes, was too weak to determine f_b accurately.[41,42] Therefore, the (110) and (200) planes were used to determine the f_a and f_b using the following equation in this article, which was first derived by Wilchinsky[43]:

$$\overline{\cos^2\Phi_{110}} = 0.692\ \overline{\cos^2\Phi_{020}} + 0.308\ \overline{\cos^2\Phi_{200}} \tag{5}$$

where

$$\overline{\cos^2\Phi} = \frac{\int_0^{\pi/2} I(\Phi)\cos^2\Phi \sin\Phi\, d\Phi}{\int_0^{\pi/2} I(\Phi)\sin\Phi\, d\Phi} \tag{6}$$

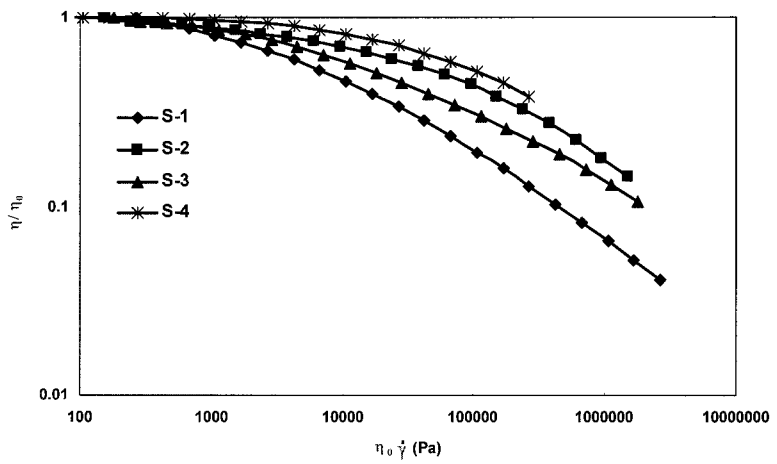

Figure 4 Vinogradov–Malkin reduced viscosity plot.

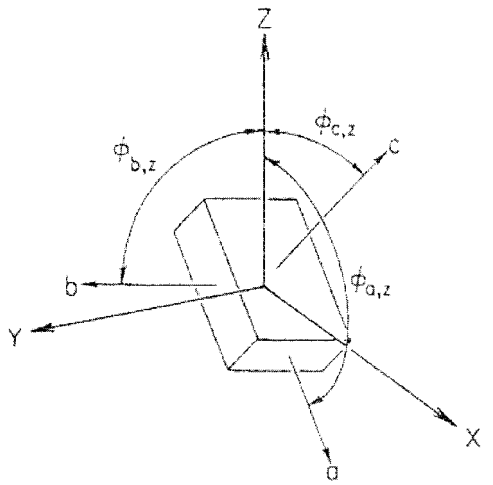

Figure 5 Orientation of unit cell of PE.

The value of f_c was then calculated using eq. (4).

For S-4, besides the orthorhombic crystal, we also attempted to calculate the orientation factor of the hexagonal phase using eqs. (3) and (6).

A Bruker AXS HI-STAR general area detector diffraction system (GADDS; Bruker Instruments, Billerica, MA), with graphite monochromatized Cu–K_α, was used to obtain the diffraction patterns of the filaments, and thus to calculate the orientation factor of each crystal plane. The intensity was corrected for background scattering, detector noise, and absorption. The method of Fujino et al.[41,42] was used to correct for overlap between various peaks. For orientated specimens, there was some anisotropy along the azimuthal angle to the amorphous halos (i.e., enhanced intensity in the region of the equatorial Bragg reflection). However, this anisotropy was relatively small. By use of the method proposed by Androsch et al.[16] the amorphous background was subtracted from the area detector data. The scattering contained in the three equatorial reflections (i.e., that attributed to the crystalline components) was thus estimated.

The birefringence of the melt-spun filaments was determined by the optical retardation method, using a Leitz (Wetzlar, Germany) polarized light microscope with a 30-order Berek compensator. At each draw-down ratio, 10 to 20 samples were measured and the results were averaged.

Engineering stress–strain measurements were made on the melt-spun filaments using an Instron tensile machine at room temperature. The gauge length was 22.5 mm and the crosshead speed was 22.5 mm/min. At each draw-down ratio, approx. 10 samples were measured. The mechanical properties, i.e., modulus, tensile strength, and elongation to break were averaged for those with the same draw-down ratio.

RESULTS

Melt spinning behavior

All of the fibers were melt spun as described. The spinline stresses for the four polymers at a 170°C melt-spinning temperature are shown in Figure 6(a) as a function of draw-down ratio V_1/V_0. Some of the filaments broke in the spinline. The maximum draw-down ratios achieved were 1305 for S-1, 470 for S-2, 539 for S-3, and 677 for S-4. The spinline stresses on the four materials at different melt temperatures are shown in Figures 6(b) and (c). Generally, the spinline stress increases monotonically with increasing draw-down ratio or with decreasing melt temperature. The values of spinline stress are of the same order of magnitude under the processing conditions investigated in this study. The spinline stresses based on melt spinning at 170°C are in the order: S-3 > S-1 > S-2 > S-4.

Crystallinity of melt-spun filament

The crystallinity of the melt-spun filaments of all four samples shows a slight increase with the draw-down ratio, as shown in Fig. 7.

X-ray diffraction

WAXD patterns of the four copolymers filaments with different draw-down ratios are shown in Figure 8. The *d*-spacings for the Bragg reflections measured with the Bruker GADDS are given in Table III, which also includes both the theoretical *d*-spacing, based on the orthorhombic unit cell with lattice parameters given by Bunn,[9] and experimental *d*-spacing given by Androsch et al.[16] for S-4. It can be clearly seen from Figure 8 that for S-1, S-2, and S-3, the crystal form can be represented by a Bunn[9] orthorhombic unit cell and the primary WAXD reflections are (110), (200), and (020). However, for S-4, we observe an intense amorphous halo on which are superimposed three Bragg reflections. The second and third reflections are identified as (110) and (200) of the orthorhombic phase. The first reflection is identified as (100) of the hexagonal unit cell, suggested by Androsch et al.[16,17] for this type of copolymers. No other crystal plane of the hexagonal crystal was observed.

Crystalline orientation factors

Using the method described in the experimental section, we calculated the orientation factors of *a*-, *b*-, and *c*-axes of the orthorhombic crystal. These are shown in Figure 9 as a function of spinline stress. For sample S-4, we also present the orientation factor of the *a*-axis of the hexagonal phase (f_{hexa}). It can be seen that for

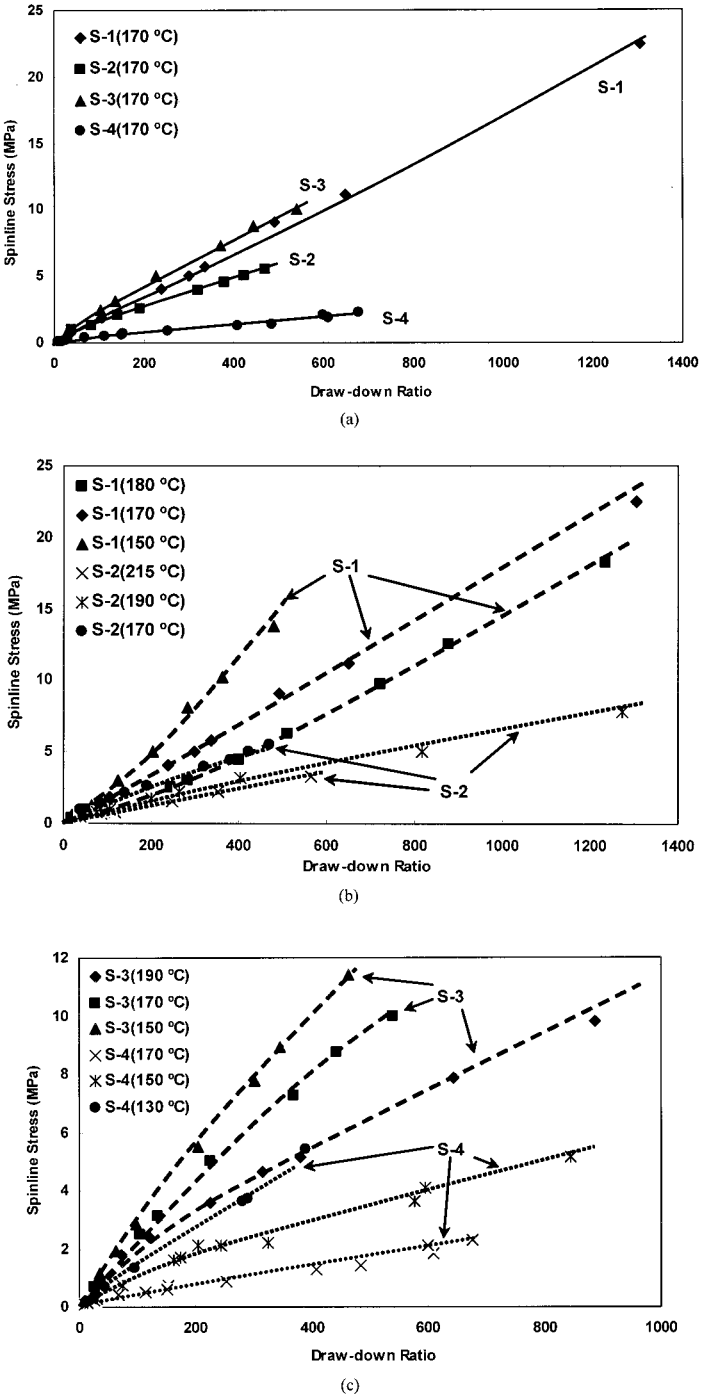

Figure 6 Spinline stresses of the melt-spun filaments as a function of draw-down ratio (V_L/V_0): (a) S-1, S-2, S-3, and S-4 at 170°C; (b) S-1 and S-2 at specific temperatures; (c) S-3 and S-4 at specific temperatures.

S-1, S-2, and S-3, with an increase of the spinline stress, f_b rapidly reaches a value of about -0.4 for S-1. For S-2 and S-3, it decreases progressively more slowly. f_a first reaches a maximum value, and then decreases, becomes 0, and eventually reaches the value of about -0.45. There is a tendency toward *c*-axis orientation with increasing the spinline stress. The tendency is the strongest in S-1 and the weakest in S-3.

The orientation behavior of S-4 seems different from that of S-1, S-2, and S-3. For the orthorhombic crystals in S-4, f_a reaches a value of about -0.3 once the filament is drawn down, which means the *a* crystallographic axis is nearly perpendicular to the fiber axis; f_b reaches a value of about -0.3; the *c* crystallographic axis, on the other hand, tends to align itself along the fiber axis and f_c reaches a value of about 0.7. For the

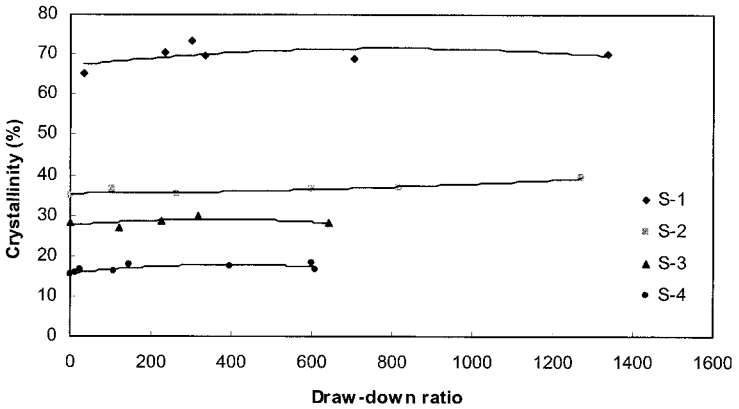

Figure 7 Crystallinity of the melt-spun filament of four samples at different draw-down ratios.

hexagonal phase, its *a*-axis tends to be perpendicular to the fiber axis and the orientation factor reaches about −0.3.

From Figure 9, we can also see the orientation factors of each polymer correlate with spinline stress independent of melt temperature.

Birefringence

The birefringence of the melt-spun filaments of the four polymers is shown as a function of spinline stress in Figure 11. If we plot the birefringence versus the draw-down ratio (Fig. 10), we obtain different curves with different processing temperatures. However, if we plot them against the spinline stress, we find these separate curves coincide.

For S-1, we observe a steep S-shape curve with a point of inflection about spinline stress $\sigma = 1.5$ MPa. For S-2 and S-3, we observe a lower sloped S-shape curve with a point of inflection about $\sigma = 3$ and 4 MPa, respectively. For S-4, we have a convex curve. All four curves show that the birefringence values increase up to a certain level and then plateau with further increasing spinline stress. The birefringence values at higher stress levels order: S-1 > S-2 > S-3 > S-4.

Mechanical properties

The typical stress–strain curves of melt-spun filaments at different draw-down ratios of four polymers are shown in Figure 12. For materials with low draw-down ratios, with increases of octene content, the stress–strain behavior changes from yielding with necking to uniform extension. S-1 shows typical necking and plastic behavior, where S-4 shows typical elastomer behavior. With an increase of melt-spinning draw-down ratio, the necking phenomenon of S-1 disappears. The stress first increases sharply with the strain in a very short range (strain < 0.1), and then it gradually increases before the filament is broken. For S-2, the mechanical behavior is similar to that of S-1. For S-3 with low draw-down ratio, it shows a slight necking behavior first, and then the stress grows gradually with the strain, similar to typical elastomer behavior. For those with high draw-down ratio, the stress simply increases with the strain. However, S-4 with high draw-down ratio shows an interesting behavior, in which stress increases with two steps: an abrupt jump after an initial slow increase.

DISCUSSION

Crystal structure

A. Muller[45,46] was the first to investigate the crystal structure of *n*-alkanes. He observed that an orthorhombic form was generally found at room temperature, but at elevated temperatures near the melting point there was a hexagonal form.[46] Bunn[47] in his subsequent studies of polyethylene, observed only the orthorhombic form. The observation of the hexagonal form for polyethylene begins with Bassett,[48] who first found it under high pressure in 1974. Five years later, Pennings[49] also observed the (100) reflection for the hexagonal form at elevated temperatures in oriented polyethylene. Recently, Tashiro et al.[50] suggested an orthorhombic-to-hexagonal phase transition for a constrained polyethylene fiber in the temperature region immediately below the melting point using a simultaneous measurement system of X-ray diffraction and Raman spectra. The hexagonal form has also been found in copolymers of polyethylene with propylene[51] and octene.[16,17,19] These authors all observed only the (100) reflection of the hexagonal form. As we know, for a perfect crystal, there should be different reflection crystal planes and those should be observed from the WAXS pattern. The reason for this may be attributable to the low order of the hexagonal crystal formed under these circumstances. Perhaps we should

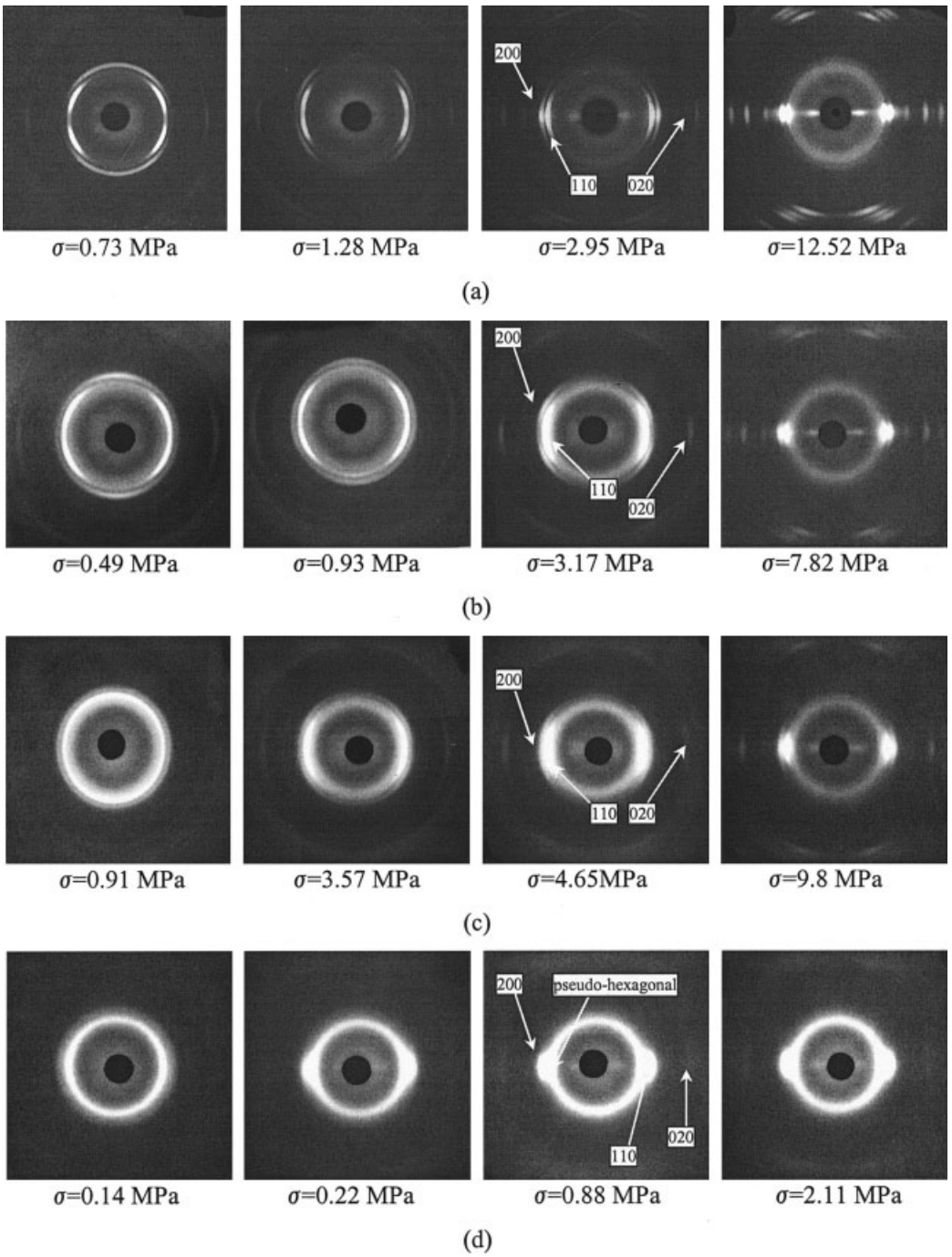

Figure 8 WAXD patterns of the melt-spun filaments of four samples at different draw-down ratios: (a) S-1; (b) S-2; (c) S-3; (d) S-4.

call it mesophase, which lies between the crystalline and the amorphous phases.

Many authors[52–54] have found that quenching isotactic polypropylene leads to a mesomorphic form in which 3/1 helices are disordered. This also happens in the melt spinning of fibers.[52,53] D. Choi and White[54] found that if lower tacticity isotactic polypropylene is melt spun, the range of conditions of forming the mesomorphic structure is increased. Introducing comonomer or disordering into polyolefins clearly leads to broader regions of formation of less-ordered structures.

Crystalline orientation factors

From Figure 9(a) and (e), we can compare our crystalline orientation factor–spinline stress plots with those of C. Choi and White[8] for HDPE (S-1). We see that both plots coincide well. At about 0.6 MPa, f_a reaches

TABLE III
Wide-Angle *d*-Spacing of Four Copolymers Used in This Study

			Polymer designation				
		Bunn[9]	S-1	S-2	S-3	S-4	Androsch[16]
Octene content (wt %)			0	15	20	38	
Crystal structure	(hkl)			Spacing (Å)			
Pseudo-hexagonal	(100)					4.534	4.52 ± 0.02
Orthorhombic	(110)	4.106	4.105	4.125	4.151	4.190	4.15 ± 0.01
	(200)	3.696	3.711	3.743	3.759	3.803	3.77 ± 0.01
	(020)	2.467	2.467	2.467			2.48

its maximum value of about 0.25 (C. Choi and White) and about 0.3 (this study), respectively; f_b decreases to its turning point of about −0.3, and then decreases slowly. At about 1.5 MPa, f_a reaches 0 in both cases. At about 3.0 MPa, f_a reaches its lowest value and then remains nearly constant; f_b equals about −0.46 and f_c equals about 0.85. It has been pointed out by Dees and Spruiell,[5] following Keller and Machin,[55,56] that based on the "row-nucleated structure," for the extremely idealized case in which the *b*-axis is perpendicular to the fiber axis, with the *a*-axis and *c*-axis randomly disposed within a plane parallel to the fiber axis, $f_a = f_c = 0.25$, $f_b = -0.5$; for the case in which the lamellae do not twist, $f_a = f_b = -0.5$ and $f_c = 1$. By comparing these values to the experimental results shown above, we can see that the orientation behavior of S-1 can be explained well using a "row-nucleated structure" model.

We can also compare the orientation factors of S-2 and S-3 fibers with those of S-1 (HDPE) from Figure 9(a)–(c). For f_a, S-1 reaches its maximum value of about 0.3 at about 0.6 MPa; S-2 reaches its maximum value of about 0.24 at about 1.0 MPa; S-3 reaches its maximum value of about 0.1 at about 1.1 MPa. For f_b, S-1 reaches about −0.4 at about 1.0 MPa, S-2 reaches about −0.4 at about 3.0 MPa, and S-3 reaches about −0.4 at about 4.0 MPa. It appears that higher stress is needed to orient the *b* crystallographic axis to be perpendicular to the fiber axis, and also for f_a to reach its maximum value. In other words, we need more stress to well establish the "row-nucleated structure" for polyethylenes with lower crystallinity. This can also be verified by checking the f_c of these three polymers. With decreasing crystallinity, f_c increases more slowly with the spinline stress. It is also interesting to compare the maximum value that f_a reaches. With increasing octene content, f_a becomes smaller.

We should further compare the orientation behavior of the orthorhombic crystal of S-4 with that of S-1 from Figure 9(a) and (d). No maximum value of f_a is observed for S-4. Instead, f_a decreases to about −0.3 at about 1.3 MPa, and then remains roughly constant. At the same stress, f_b decreases to about −0.3 and f_c increases to about 0.6. The lowest value that f_a and f_b can reach is about −0.35. These values are higher than −0.46, which S-1 has reached. The highest value that f_c reaches is about 0.7, which is lower than that S-1 achieves. From these values, we may conclude that it is harder to orient the *c*-axis of S-4 to be parallel to the fiber axis, the *a*-axis and *b*-axis of S-4 to be perpendicular to the fiber axis, than the axes of S-1. The orientation behavior of S-4 seems different from that of S-1 and cannot be explained by "row-nucleated structure." We may infer that S-4 has a different type of crystalline morphology from that of the other three samples. Bensason et al.[13] classified the copolymers into four different types on the basis of correlations between their morphologies and density/crystallinity, which depends on the comonomer concentration. According to their classification, S-4 has a granular, nonlamellar morphology. Fringed micellar or bundled crystals are thus inferred. If that is true, we can conclude that once the filament of S-4 is melt spun, the *c*-axis of the crystal will tend to orient along the fiber axis, whereas the *a*-axis and *b*-axis tend to remain perpendicular to the fiber axis.

Birefringence

Birefringence in fibers, following Hermans et al.,[57] and later Stein and Norris,[58] may be expressed as follows:

$$\Delta n = \Delta n_{\text{cryst}} + \Delta n_{\text{amorph}} + \Delta n_{\text{form}} \tag{6a}$$

$$\Delta n = X f_{\text{cryst}} \Delta^{\circ}_{\text{cryst}} + (1 - X) f_{\text{amorph}} \Delta^{\circ}_{\text{amorph}} + \Delta n_{\text{form}} \tag{6b}$$

where X is the crystallinity; f_{cryst} and f_{amorph} are crystalline and amorphous orientation factors; $\Delta^{\circ}_{\text{cryst}}$ and $\Delta^{\circ}_{\text{amorph}}$ are intrinsic birefringence of crystalline and amorphous phases, respectively; and Δn_{form} is form birefringence. For simplification, we take $\Delta^{\circ}_{\text{amorph}}$ to be equal to $\Delta^{\circ}_{\text{cryst}}$, which is 0.0585.[59] We also consider the $\Delta^{\circ}_{\text{amorph}}$ and $\Delta^{\circ}_{\text{cryst}}$ of the four polymers to be the same. The crystallinity, as we have mentioned before, is

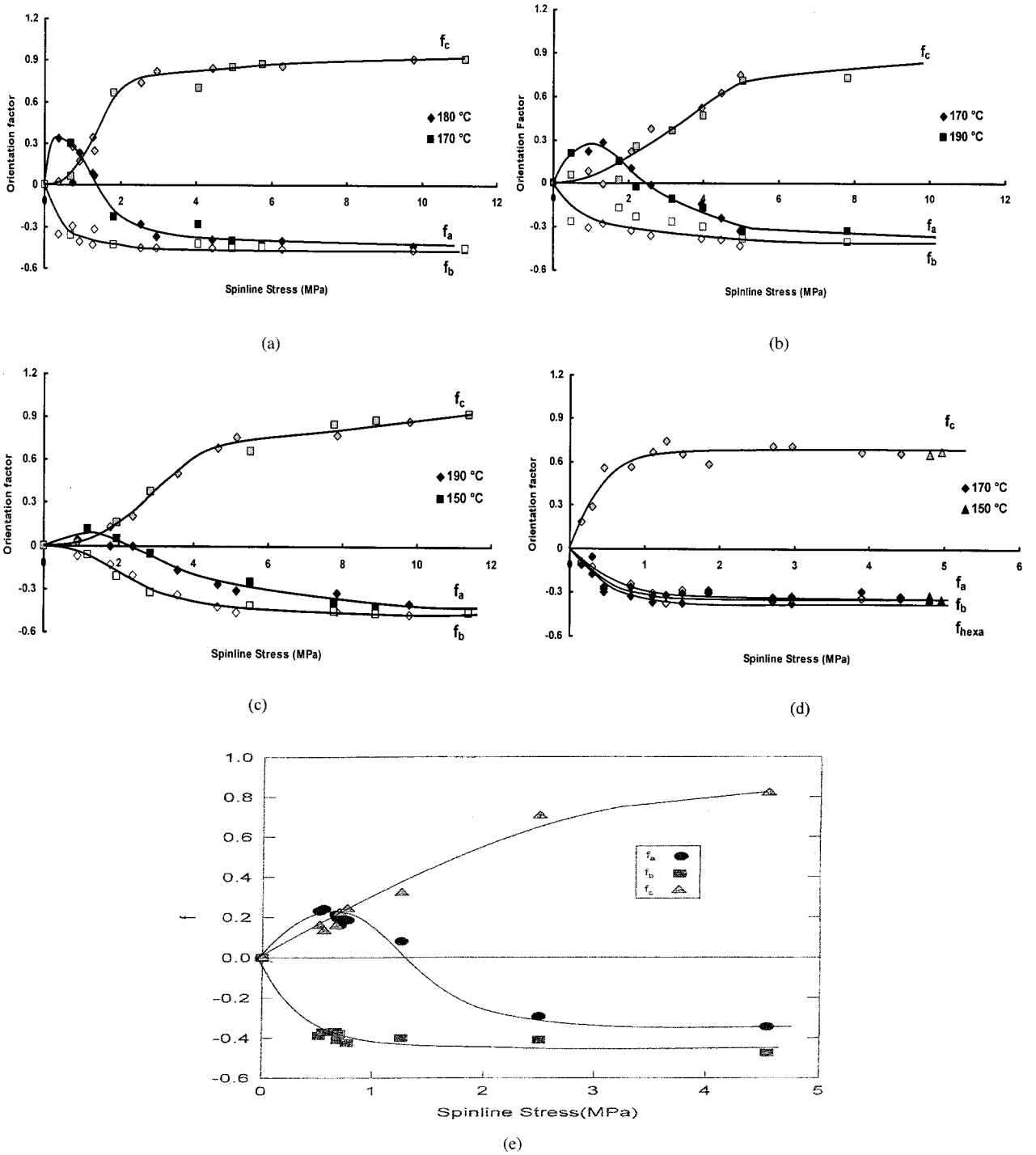

Figure 9 Orientation factor of melt-spun filaments as a function of spinline stress: (a) S-1; (b) S-2; (c) S-3; (d) S-4; (e) C. Choi and White's data on HDPE.

taken as constant with different draw-down ratios. Δn_{form} is usually neglected.

Introducing our data for S-1, S-2, S-3, and S-4, we find that for S-1, f_{amorph} is near zero or negative; S-2 is about 0.08; S-3 is about 0.12; and S-4 is about 0.2. It seems that f_{amorph} increases with decreasing crystalline content.

Mechanical properties

The modulus, tensile strength, and elongation to break of the filaments of the four materials with different birefringences are shown in Figures 13, 14, and 15, respectively. Figure 13 shows that the moduli of S-1,

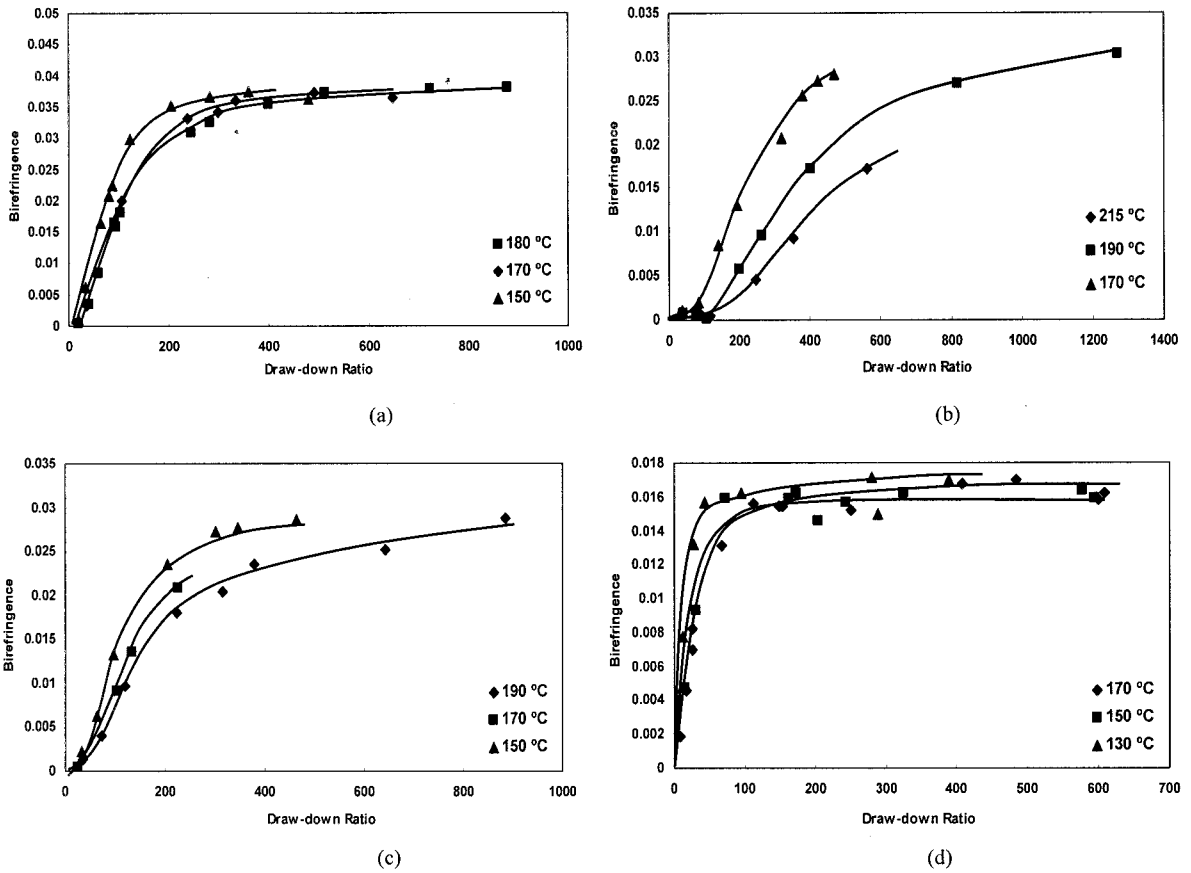

Figure 10 Birefringence of melt-spun filaments as a function of draw-down ratio: (a) S-1; (b) S-2; (c) S-3; (d) S-4.

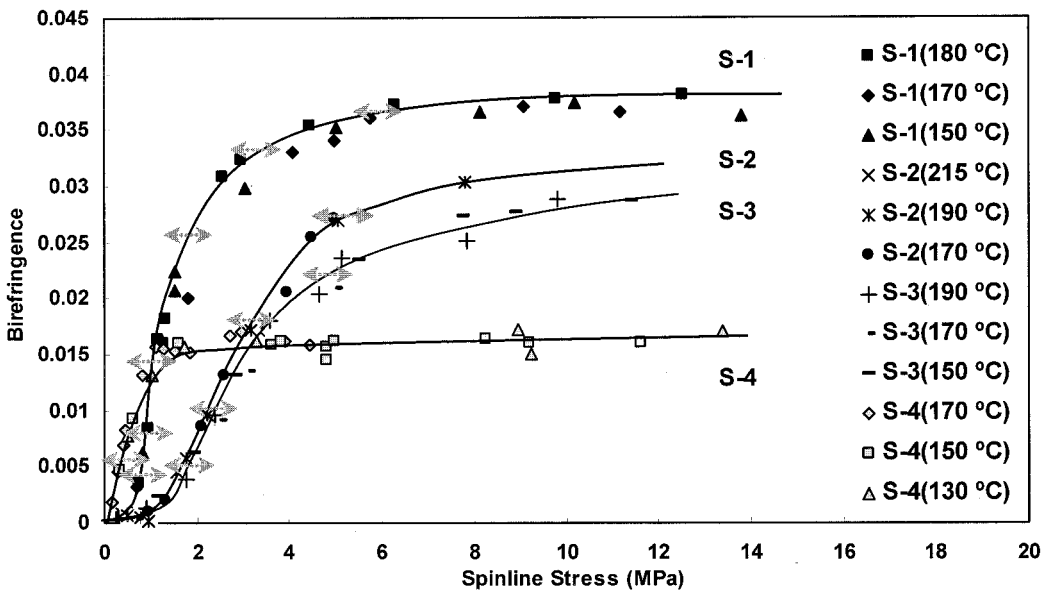

Figure 11 Birefringence of melt-spun filaments as a function of spinline stress.

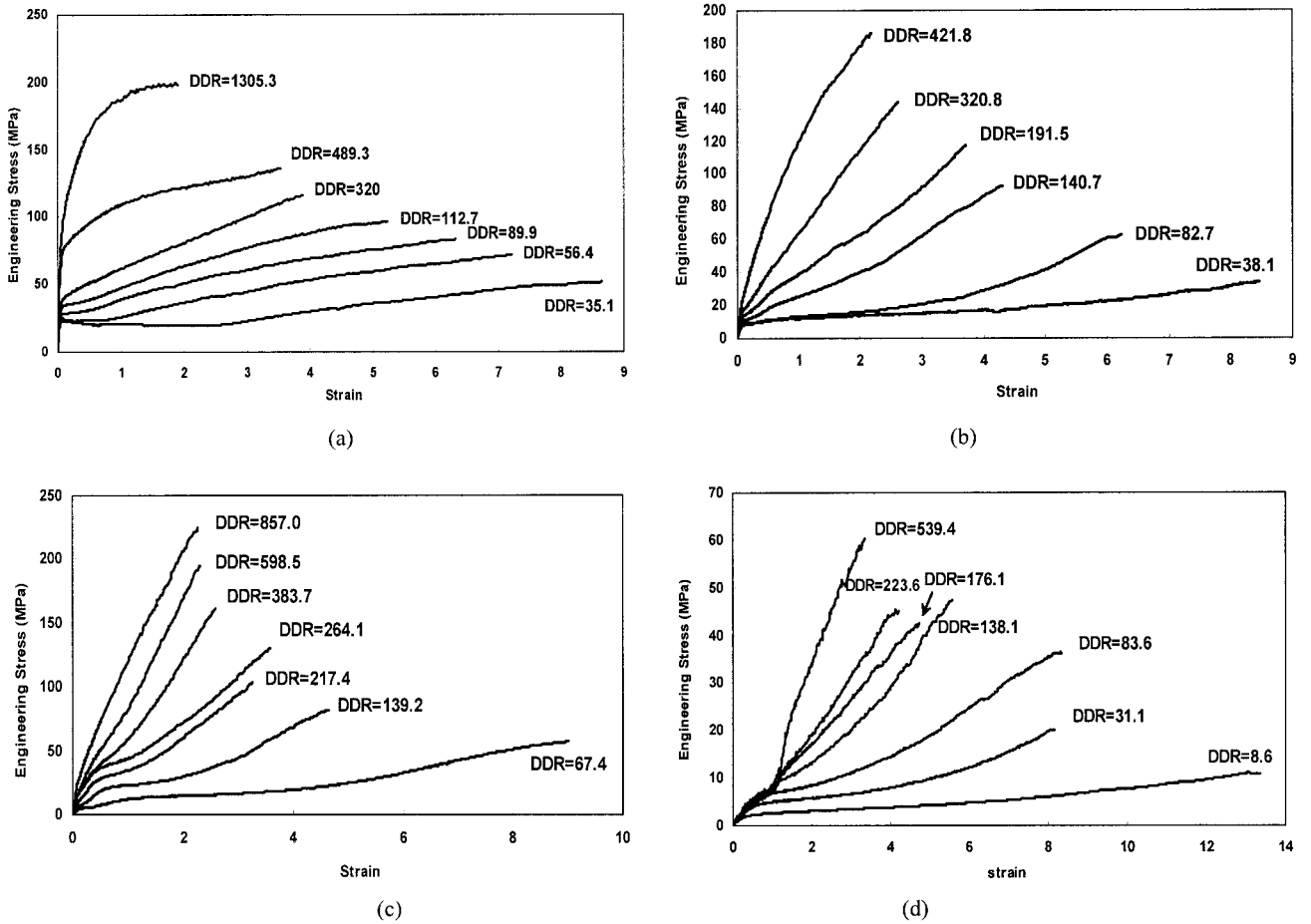

Figure 12 Engineering stress–strain curve for melt-spun filaments with different draw-down ratios: (a) S-1; (b) S-2; (c) S-3; (d) S-4.

S-2, and S-3 increase with an increase of birefringence; however, that of S-4 seems to remain unchanged. The modulus decreases with the increase of the content of octene at the same birefringence. Because the octene level correlates with the crystallinity of the material, the modulus is thus also proportional to the crystallinity of the material. It seems we can thus correlate the modulus with the crystallinity and birefringence of the material. However, no exact relationship could be found at this point.

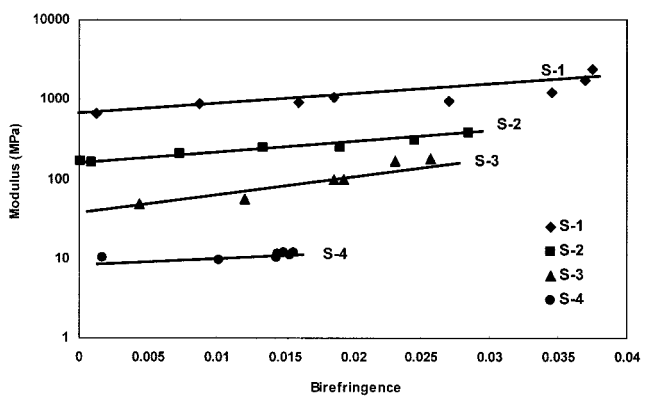

Figure 13 Modulus for melt-spun filaments of four copolymers versus birefringence.

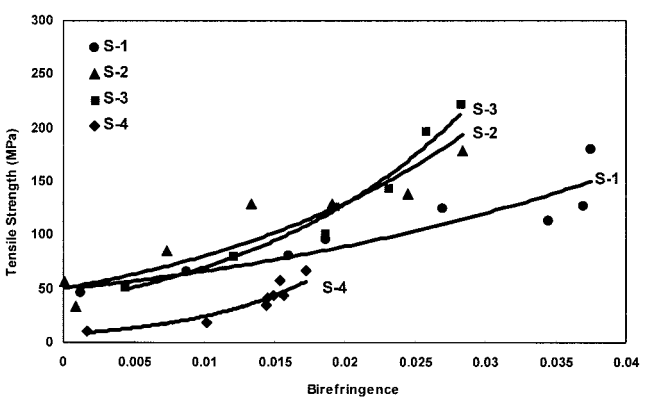

Figure 14 Tensile strength for melt-spun filaments of four copolymers versus birefringence.

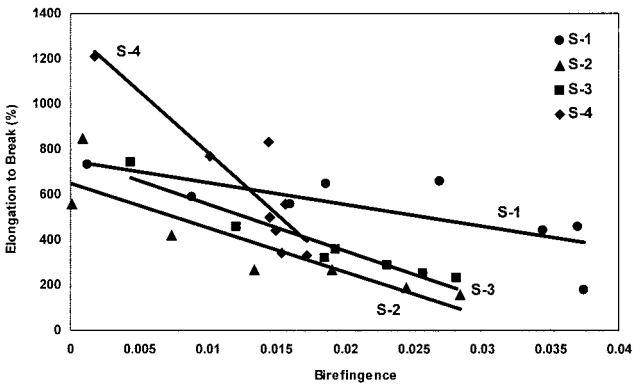

Figure 15 Elongation to break for melt-spun filaments of four copolymers versus birefringence.

The tensile strength of the filament of four materials also increases with the birefringence as shown in Figure 14. The tensile strength of S-3 is higher than the more crystalline one. This agrees with the manufacturer's specifications. The elongation to break decreases with increase of birefringence for all four materials.

CONCLUSIONS

The level of crystallinity, crystal structure, orientation factor of crystal, birefringence, and mechanical property of filaments of poly(ethylene-*co*-octene) with various octene contents were investigated. With an increase of octene content, the crystallinity decreases for the four polymers studied, and so does the melting point. The crystallinities of the four types of polymer filaments show a slight increase with draw-down ratio. An orthorhombic crystal structure for all four polymer filaments was observed, although a hexagonal mesophase structure was found to be dominant for the copolymer with the highest octene content. The orientation factors of the *a*, *b*, and *c* crystalline axes were determined. The crystal orientation behavior of S-1, S-2, and S-3 can be explained on the basis of "row-nucleated structure" model. However, that of S-4 seems different and can perhaps be explained using the granular, nonlamellar morphology. The birefringence of the filaments of four materials first increases with the spinline stress, then levels off. The sequence of the birefringence is according to the following order: S-1 > S-2 > S-3 > S-4 at the same spinline stress. The mechanical behavior of four polymers showed that increasing the birefringence will increase the modulus and tensile strength, while decreasing the elongation to break. Also, decreasing the crystallinity decreases the modulus of the filament.

The authors thank Dow Chemical, DuPont Dow, and Equistar for supplying the polymers.

References

1. Ziabicki, A.; Kedzierska, K. J Appl Polym Sci 1962, 6, 361.
2. Katayama, K.; Amano, T.; Nakamura, K. Kolloid Z Z Polym 1968, 226, 125.
3. Kitano, T.; Ohya, S.; Furukawa, J.; Yamashita, S. J Polym Sci Part B: Polym Phys 1973, 11, 1091.
4. Abbott, L. E.; White, J. L. J Appl Polym Sci Appl Polym Symp 1973, 20, 247.
5. Dees, J. R.; Spruiell, J. E. J Appl Polym Sci 1974, 18, 1053.
6. White, J. L.; Dharod, K. C.; Clark, E. S. J Appl Polym Sci 1974, 18, 2539.
7. Nadkarni, V. M.; Schultz, J. M. J Polym Sci Part B: Polym Phys 1977, 15, 2151.
8. Choi, C. H.; White, J. L. Int Polym Process 1998, 13, 78.
9. Bunn, C. W. Trans Faraday Soc 1939, 35, 482.
10. Mathot, V. B. F.; Pijpers, M. J. F. J Appl Polym Sci 1990, 39, 979.
11. Defoor, F.; Groeninck, G.; Reynaers, H.; Schouterden, P.; Van der Heijden, B. Macromolecules 1993, 26, 2575.
12. Minick, J.; Moet, A.; Hiltner, A.; Baer, E.; Chum, S. P. J Appl Polym Sci 1995, 58, 1871.
13. Bensason, S.; Minick, J.; Moet, A.; Chum, S.; Hiltner, A.; Baer, E. J Polym Sci Part B: Polym Phys 1996, 34, 1301.
14. Bensason, S.; Stepanov, E. V.; Chum, S.; Hiltner, A.; Baer, E. Macromolecules 1997, 30, 2436.
15. Akpalu, Y.; Kielhorn, L.; Hsiao, B. S.; Stein, R. S.; Russell, T. P.; van Egmond, J.; Muthukumar, M. Macromolecules 1999, 32, 765.
16. Androsch, R.; Blackwell, J.; Chaulun, S. N.; Wunderlich, B. Macromolecules 1999, 32, 3735.
17. Androsch, R. Polymer 1999, 40, 2805.
18. Androsch, R.; Wunderlich, B. Macromolecules 1999, 32, 7238.
19. Androsch, R.; Wunderlich, B. Macromolecules 2000, 33, 9076.
20. Simanke, A. G.; Alamo, R. G.; Galland, G. B.; Mauler, R. S. Macromolecules 2001, 34, 6959.
21. Androsch, R.; Wunderlich, B.; Wu, T.; Wutzl, A. J Polym Sci Part B: Polym Phys 2002, 40, 1223.
22. Keating, M. Y.; Lee, I. H. J Macromol Sci Phys 1999, B38, 379. [Product information from Equistar Chemicals LP, Dow Chemical Company, and Dupont Dow Elastomers Corp.]
23. Cox, W. P.; Merz, E. H. J Polym Sci 1958, 28, 619.
24. Wales, J. L. S.; DenOtter, I. L. Rheol Acta 1970, 9, 115.
25. Wang, J.; Knox, J. R.; Porter, R. S. J Polym Sci Polym Phys Ed 1978, 16, 1709.
26. Kitano, T.; Nishimura, T.; Kataoka, T.; Sakai, T. Rheol Acta 1980, 19, 671.
27. Steller, R. Rheol Acta 1985, 24, 541.
28. Venkatraman, S.; Okano, M.; Nixon, A. Polym Eng Sci 1990, 30, 308.
29. Garcia-Franco, C. A. Rheol Acta 1999, 38, 34.
30. Wood-Adams, P. M. J Rheol 2001, 45, 203.
31. Benoit, D. J Rheol 2002, 46, 1155.
32. Wood-Adams, P. M.; Dealy, J. M.; deGroot, A. W.; Redwine, O. D. Macromolecules 2000, 33, 7489.
33. Raju, V. R.; Smith, G. G.; Martin, G.; Knox, J. R.; Graessley, W. W. J Polym Sci Polym Phys Ed 1979, 17, 1183.
34. Vinogradov, G. V.; Malkin, A. Y. J Polym Sci A-2 1966, 4, 135.
35. Onogi, S.; Masuda, T.; Shiga, I.; Costaschuk, F. M. Appl Polym Symp 1972, 20, 37.
36. Minoshima, W.; White, J. L.; Spruiell, J. E. Polym Eng Sci 1980, 20, 1166.
37. Yamane, H.; White, J. L. Polym Eng Rev 1982, 2, 167.
38. Hermans, P. H.; Platzek, P. Kolloid Z 1939, 88, 68.
39. Muller, F. H. Kolloid Z 1941, 95, 138.
40. Stein, R. S. J Polym Sci 1958, 31, 327.
41. Desper, C. R.; Stein, R. S. J Appl Phys 1966, 37, 3990.

42. Fujino, K.; Kawai, H.; Oda, T.; Maeda, H. In: Proceedings of the Fourth International Congress on Rheology; Lee, E. H., Ed.; Interscience: New York, 1963; Vol. 3, p. 501.
43. Wilchinsky, Z. W. J Appl Phys 1960, 31, 1969.
44. Hermans, J. J.; Hermans, P. H.; Vermaas, D.; Weidinger, A. Rec Trav Chim 1946, 65, 427.
45. Muller, A. Proc R Soc London Ser A 1928, 120, 437.
46. Muller, A. Proc R Soc London Ser A 1932, 138, 514.
47. Bunn, C. W.; Alcock, T. C. Trans Faraday Soc 1945, 41, 317.
48. Bassett, D. C.; Block, S.; Piermarini, G. J. J Appl Phys 1974, 45, 4146.
49. Pennings, A. J.; Zwijnenburg, A. J Polym Sci Part B: Polym Phys 1979, 17, 1011.
50. Tashiro, K.; Kariyo, S. J Polym Sci Part B: Polym Phys 2002, 40, 495.
51. Ruiz de Ballesteros, O.; Auriemma, F.; Guerra, G.; Corradini, P. Macromolecules 1996, 29, 7141.
52. Natta, G.; Peraldo, M.; Corradini, P. Rend Accad Naz Lincei 1959, 26, 14.
53. Nadella, H. P.; Henson, H. M.; Spruiell, J. E.; White, J. L. J Appl Polym Sci 1977, 21, 3003.
54. Choi, D.; White, J. L. Int Polym Process 2000, 15, 398.
55. Keller, A.; Machin, M. J. J Macromol Sci Phys 1967, B1, 41.
56. Hill, M. J.; Keller, A. J Macromol Sci Phys 1969, B3, 153.
57. Hermans, P. H.; Hermans, J. J.; Vermaas, D.; Weidinger, A. J Polym Sci 1948, 3, 1.
58. Stein, R. S.; Norris, F. H. J Polym Sci 1956, 21, 381.
59. Bunn, C. W.; deDaubeny, R. Trans Faraday Soc 1954, 50, 1173.